

# Thermal Dileptons from $\pi - \rho$ Interactions in a Hot Pion Gas

R. Baier<sup>1</sup>, M. Dirks<sup>1</sup> and K. Redlich<sup>2,3</sup>

<sup>1</sup>*Fakultät für Physik, Universität Bielefeld, D-33501 Bielefeld, Germany*

<sup>2</sup>*Institute for Theoretical Physics, University of Wrocław,  
 PL-50204 Wrocław, Poland*

<sup>3</sup>*GSI, PF 110552, D-64220 Darmstadt, Germany*

## Abstract

A systematic study of low mass dilepton production from  $\pi - \rho$  interactions in a hot medium is presented. Applying finite temperature perturbation theory the dilepton rate, respectively the virtual photon rate, is computed up to order  $g_\rho^2$ . For dilepton masses below the  $\rho$  the two-body reactions  $\pi\pi \rightarrow \rho\gamma^*$ ,  $\pi\rho \rightarrow \pi\gamma^*$ , and the decay process  $\rho \rightarrow \pi\pi\gamma^*$  give significant contributions. Non-equilibrium contributions to the thermal rate are estimated, including the modification of the particle distribution function with non-zero pion chemical potential. The comparison of the dilepton rate with the recent data measured in nucleus-nucleus collisions at SPS energy by the CERES Collaboration is also performed. It is shown that the additional thermal dileptons from  $\pi - \rho$  interactions can partially account for the excess of the soft dilepton yield seen experimentally.

# 1 Introduction

Dilepton production is one of the interesting tools to study collective effects in strongly interacting matter produced in ultrarelativistic heavy ion collisions [1, 2, 3, 4]. This is particularly evident from the recent CERN experimental data at SPS collision energy. A significant enhancement of the dilepton spectrum measured in A-A collisions as compared with p-p and p-A collisions is reported. Two experiments, CERES/NA45 [5] and HELIOS/3 [6] have measured dileptons in the low mass range in S-Au, Pb-Au and S-W collisions respectively. Both these experiments have reported the excess of dileptons with invariant masses between 0.25 and 1 GeV in A-A nuclear collisions, compared to expected [5] or measured [6] spectra in p-A collisions.

These remarkable results indicate the appearance of collective phenomena in heavy ion collisions, like thermalization of the medium after the collision. Since the temperatures are not yet to be expected as high, in particular the reactions involving pions and rho mesons are important and have to be considered. In the kinematical window of low mass dileptons pion annihilation with the  $\rho$  in the intermediate state is a basic source of thermal dileptons, also responsible for the low mass dilepton enhancement reported by the CERN experiments. Indeed, recent theoretical calculations show that close to the  $\rho$  peak the thermal production rate due to pion annihilation is compatible with the experimental data [7, 8]. However, neither the size of the excess below the  $\rho$  peak nor the shape of the distribution is quantitatively explained by this contribution alone. In a thermal medium, however, the partial restoration of chiral symmetry in hot and dense hadronic matter may modify the properties of vector mesons especially their mass or decay width [9, 10]: in Ref. [7] it is shown that thermal dilepton production due to the pion annihilation process together with the assumption of a decreasing rho meson mass leads to a quantitative explanation of the enhancement of the low-mass dileptons observed by the CERES and by the HELIOS/3 experiments.

The above results together with previous theoretical studies [11, 12, 13] suggest the importance of pion scattering in a medium as a source of soft dileptons. In a thermal medium, however,  $\pi^+\pi^- \rightarrow e^+e^-$  is not the only process which has to be considered. For example the contribution from the two-body reaction  $\pi^+\pi^- \rightarrow \rho\gamma^* \rightarrow \rho e^+e^-$  does not have a kinematical threshold at  $2m_\pi$ , and therefore certainly dominates the basic pion annihilation process for dilepton masses  $M \simeq 2m_\pi$ . This example indicates, that a more complete analysis of the low mass dilepton spectrum originating from a possible thermal medium, requires further considerations.

Previous calculations of the thermal rate of emission of direct, i.e. real, photons with energies less than 1 GeV have shown that there are two contributing reactions involving a neutral  $\rho$ : the annihilation process  $\pi^+\pi^- \rightarrow \rho^0\gamma$  and Compton like scattering  $\pi^\pm\rho^0 \rightarrow \pi^\pm\gamma$  [14]. Both contribute to dilepton production, where the real photon is replaced by a virtual one. The importance of two-body processes for low mass dileptons has also been stressed in the case of production from the quark-gluon plasma [15].

In this paper we compute the contributions to the dilepton production rate from  $\pi - \rho$  interactions for invariant masses up to the  $\rho$  peak. In sect. 2, after shortly treating the  $\pi^+\pi^- \rightarrow \gamma^*$  Born rate, we discuss the "real"  $2 \rightarrow 2$  and  $\rho \rightarrow \pi\pi\gamma^*$  reactions, at the two-loop level of the virtual photon selfenergy. Also the "virtual" two-loop corrections to the Born rate are derived. Sect. 3 extends the estimates of the dilepton rate taking into account out of equilibrium effects

by introducing the pion chemical potential. Finally, in sect. 4 we compare the dilepton rate with experimental data [5] in the low mass region.

## 2 Dilepton production and $\pi - \rho$ interactions

The thermal dilepton production rate is considered in lowest order of the electromagnetic coupling. First, the medium is taken at rest. The rate per unit space-time volume,  $dR \equiv dN/d^4x$ , is related to the absorptive part of the photon self-energy tensor  $\Pi_{\mu\nu}$  [2, 11, 16, 17]. For lepton pairs of invariant mass  $M$ , energy  $q_0$  and momentum  $\vec{q}$  the relation is

$$\frac{dR}{dM^2 d^3q/q_0} = -\frac{\alpha}{24\pi^4 M^2} n(q_0) \text{Im}\Pi_\mu^\mu(q_0, \vec{q}), \quad (2.1)$$

where  $n$  is the Bose distribution function at temperature  $T = 1/\beta$  (cf. Appendix A). The tensor is constrained by current conservation  $q_\mu \Pi_\nu^\mu(q) = 0$ .

We adopt the real-time formulation of finite temperature field theory to evaluate  $\text{Im}\Pi_\mu^\mu$ . Using the Keldysh variant (with time path-parameter  $\sigma = 0$  [18, 19, 20]) the following useful relation holds in terms of the photon-selfenergy matrix  $\Pi_{ab}^\gamma$ ,

$$\text{Im}\Pi_\mu^\mu(q_0, \vec{q}) = \frac{1}{2n(q_0)} i\Pi_{12}^\gamma(q_0, \vec{q}). \quad (2.2)$$

### 2.1 Born rate

In order to clarify the notation we give the one-loop expression for  $\Pi_{12}^\gamma$ . With the momentum labels indicated in Fig. 1 this pion-loop contribution with the temperature-dependent propagators (A.1), summarized in Appendix A, reads

$$i\Pi_{12}^\gamma(q_0, \vec{q}) = -(-ie)^2 \int \frac{d^4p}{(2\pi)^4} (p+p')^2 iD_{12}(p) iD_{21}(p'), \quad (2.3)$$

where  $p' = p - q$ .

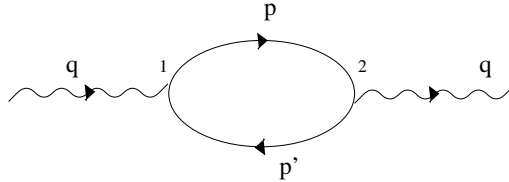


Figure 1: *One-loop photon selfenergy diagram. The solid line denotes the pion*

Using the equilibrium distributions one recovers the standard expression for the Born term  $\pi^+\pi^- \rightarrow \gamma^* \rightarrow l^+ l^-$ . For masses  $M$  near the  $\rho$  it is appropriate [11] to implement VDM and to insert the pion electromagnetic formfactor  $F_\pi$ ,

$$|F_\pi(M)|^2 = \frac{m_\rho^4}{(M^2 - m_\rho^{*2})^2 + \Gamma_\rho^2 m_\rho^2}, \quad (2.4)$$

into the production rate. For our numerical analysis the parameters are chosen as  $m_\rho = 0.775$  GeV,  $m_\rho^* = 0.761$  GeV and  $\Gamma_\rho = 0.118$  GeV in agreement with the measured pion electromagnetic form factor [11]. We do not consider the possibility of medium dependent resonance parameters, as done in [7]. Also contributions due to the  $A1$  resonance [21] are neglected.

For soft dileptons with invariant masses  $M < m_\rho$  the mass distribution per unit space time volume is obtained within a very good approximation from the rate with the heavy photon taken at rest with respect to the medium (also kept at rest) [3, 10]

$$\frac{dN}{dM^2 d^4x} \simeq 4\pi T^2 \left(\frac{\pi M}{2T}\right)^{1/2} \frac{dR}{dM^2 d^3q/q_0} \Big|_{\vec{q}=0}, \quad (2.5)$$

where the Born rate for  $M \simeq m_\rho$ , with the Boltzmann approximation of the pion distribution, has the following simple form,

$$\frac{dR^{Born}}{dM^2 d^3q/q_0} \Big|_{\vec{q}=0} = \frac{\alpha^2}{96\pi^4} |F_\pi(M)|^2 \exp(-M/T). \quad (2.6)$$

The more complete expression for the Born contribution with quantum statistics and arbitrary heavy photon momentum is, however, also well known in the literature (see e.g. [4]). It will be used in the following numerical estimates. Throughout the paper we neglect the pion mass (except for the numerical analysis of the Born rate for  $M < m_\rho$ ), and the masses of the leptons. Because of the many uncertainties we believe that these approximations are very well justified.

Taking into account out of equilibrium effects in determining the rates, the expression (2.6) is multiplied by a factor

$$1 + 2\delta\lambda, \quad (2.7)$$

with  $\delta\lambda = \lambda - 1$  in terms of the fugacity  $\lambda$  (cf. Appendix A). This first approximation, i.e. staying near equilibrium for  $\delta\lambda \ll 1$ , and neglecting more complicated dependences, should indicate the possible increase ( $\lambda > 1$ ) or the decrease ( $\lambda < 1$ ) of the dilepton rate due to non-equilibrium effects.

## 2.2 Two-loop contributions

The interaction of the charged pions with the neutral massive rho meson field  $\rho_\mu$  and the electromagnetic potential  $A_\mu$  is described by the Lagrangian [14]

$$L = |D_\mu \Phi|^2 - \frac{1}{4} \rho_{\mu\nu} \rho^{\mu\nu} + \frac{1}{2} m_\rho^2 \rho_\nu \rho^\nu - \frac{1}{4} F_{\mu\nu} F^{\mu\nu} \quad (2.8)$$

where  $D_\mu \equiv \partial_\mu - ieA_\mu - ig_\rho \rho_\mu$  is the covariant derivative,  $\Phi$  is the complex pion field,  $\rho_{\mu\nu}$  is the rho and  $F_{\mu\nu}$  is the photon field strength tensor. As is well known, the  $\rho\pi\pi$  coupling is rather large  $g_\rho^2/4\pi \simeq 2.9$ ; nevertheless we attempt an effective perturbative treatment up to two-loops. However, no resummation of high temperature effects, e.g. comparable to the hard thermal loop expansion for QCD [22, 23], is implemented in our approach, which maybe compared with an analogous fixed-order calculation for dilepton production from a quark-gluon plasma [24].

From the Lagrangian (2.8) and using the closed-time-path formalism [18, 19] we calculate the dilepton production rate produced in a thermal pionic medium at the two-loop level. Typical diagrams are shown in Figs. 2 and 3. The two tadpole diagrams of  $O(g_\rho^2)$  are not included, since they do not contribute to the discontinuity of the photon selfenergy (2.2).

### 2.2.1 Real $\rho^0$ processes

The processes involving real  $\rho^0$ 's, namely  $\pi\pi \rightarrow \rho\gamma^*$ ,  $\pi\rho \rightarrow \pi\gamma^*$  and  $\rho \rightarrow \pi\pi\gamma^*$ , are expected to be important for dilepton masses  $M$  below the  $\rho$ -peak. These contributions are obtained by cutting the two-loop diagrams (Figs. 2 and 3) such that the  $\rho$  is put on-mass shell.

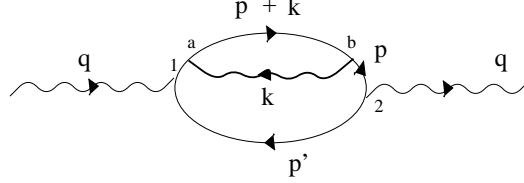


Figure 2: *Two-loop diagram: selfenergy insertion. The labels  $a, b = 1, 2$  denote the type of  $\pi\rho$  vertex. The solid line with momentum label  $k$  corresponds to the  $\rho$*

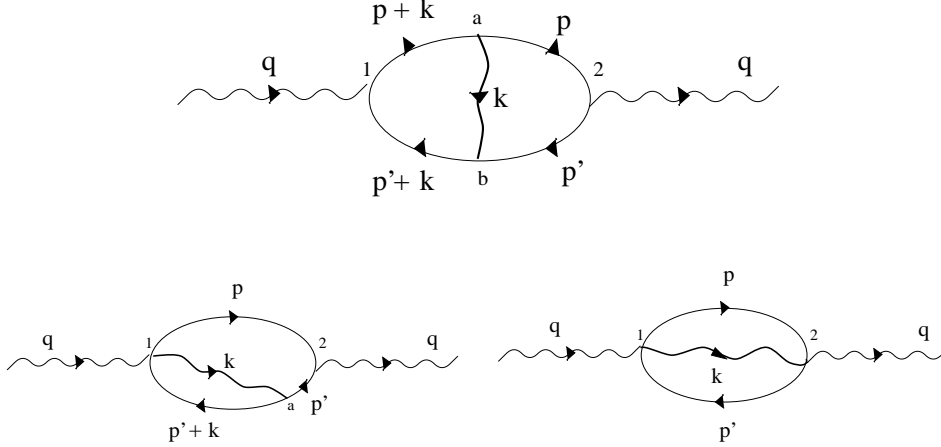


Figure 3: *Two-loop diagrams: vertex type corrections*

We start to discuss explicitly the contribution from the diagram shown in Fig. 2, where the selfenergy correction  $\delta D_{12}(p)$  is inserted into the pionline with momentum  $p$ . The expression for  $\delta D_{12}(p)$  is derived in Appendix B using the Dyson equation.

In this section we assume (thermal and chemical) equilibrium distributions (A.3), and consequently we use  $\delta D_{12}^{eq}(p)$  given in (B.5). The discussion of out of equilibrium effects in the  $\gamma^*$  rate is postponed to sect. 3.

Using the second term of (B.5) we calculate the "real" correction to (2.3)

$$i\delta\Pi_{12}^{\gamma,SE}(q^0, \vec{q}) = -(-ie)^2 \int \frac{d^4p}{(2\pi)^4} (p+p')^2 \mathbf{P} \left( \frac{1}{p^2} \right)^2 (-i\Pi_{12}(p)) iD_{21}(p'), \quad (2.9)$$

where the pion selfenergy  $i\Pi_{12}(p)$  at one-loop order due to  $\pi\rho$  interactions (2.8) is given by (cf. B.6 and C.2),

$$i\Pi_{12}(p) = g_\rho^2 \int \frac{d^4k}{(2\pi)^4} (2p+k)^\sigma \left( -g_{\sigma\tau} + \frac{k_\sigma k_\tau}{m_\rho^2} \right) (2p+k)^\tau D_{12}(p+k) D_{21}(k). \quad (2.10)$$

We note that in (2.9) we only keep the real  $\rho^0$  contributions.

Inserting the propagators (A.1) with (A.9) it is convenient to separate the different kinematical configurations, which appear due to the presence of the sign function in (A.9). We consider in more detail the process of  $\rho$ -emission, i.e.  $\pi(p_+) + \pi(p_-) \rightarrow \rho(k) + \gamma^*(q)$ , where we relabel to momenta of Fig. 2 as:  $p' \rightarrow -p_-$ ,  $p \rightarrow p_+ - k$ , and introduce (positive) energies  $k^0 = E_\rho$ ,  $p_-^0 = E_-$ ,  $p_+^0 = E_+$ . We find the following contribution to  $i\delta\Pi_{12}^{SE}$  of (2.9),

$$+ 4e^2 g_\rho^2 \int \frac{d^3 p_+}{(2\pi)^3 2E_+} n(E_+) \int \frac{d^3 p_-}{(2\pi)^3 2E_-} n(E_-) \int \frac{d^3 k}{(2\pi)^3 2E_\rho} (1 + n(E_\rho)) \\ \times (2\pi)^4 \delta^4(p_+ + p_- - k - q) (2p_- - q)^2 \mathbf{P} \left( \frac{1}{(p_+ - k)^2} \right)^2 p_+^\sigma \left( -g_{\sigma\tau} + \frac{k_\sigma k_\tau}{m_\rho^2} \right) p_+^\tau, \quad (2.11)$$

expressed in a form familiar from kinetic theory [2]: it consists of the square of the matrix element for the two-body process  $\pi\pi \rightarrow \rho\gamma^*$ , here to one of the exchange diagrams plotted in Fig. 4, with the integration over the phase-space of the participating pions and the  $\rho$ -meson properly weighted by the thermal distribution functions  $n(E)$ . Next we also integrate with respect to the photon momentum  $\vec{q}$  as described in Appendix D.

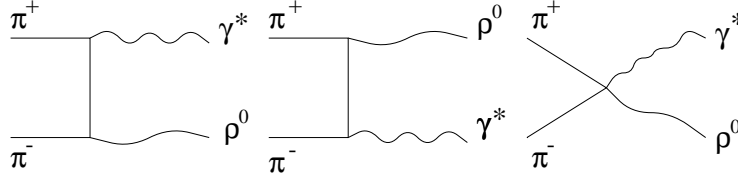


Figure 4: *Matrix elements for the process  $\pi\pi \rightarrow \rho\gamma^*$  arising from cutting the two-loop diagrams*

An analogous, straightforward treatment gives the corresponding contributions to the real  $\rho^0$  processes from the two-loop vertex type diagrams of Fig. 3. Finally we sum all these contributions, including those obtained by interchanging momenta, like the selfenergy contribution of (2.9), but interchanging  $p$  and  $p'$  in Fig. 2.

As a check the same final result is obtained when the square of the sum of the three matrixelements illustrated in Fig. 4 is taken. This approach has e.g. the advantage that current conservation is rather easily checked on the level of these matrixelements.

Here we quote the result. Mainly for simplicity we use the Boltzmann approximation which amounts to underestimate the dilepton rate: in this limit we replace e.g. in (2.11)  $n(E_+)n(E_-) \rightarrow \exp(-E_+ - E_-)/T$ , and neglect stimulated emission,  $1 + n(E_\rho) \simeq 1$ . The dilepton rate due to the real  $\rho^0$  processes is best expressed using the Mandelstam variables defined in (D.4); together with the kinematical approximations discussed in Appendix D, we obtain for the dilepton mass range  $M \leq m_\rho$ ,

$$\frac{dN^{\text{real}}}{dM^2 d^4x} \simeq \frac{\alpha^2 g_\rho^2 / 4\pi}{24\pi^4 M^2} \sqrt{\frac{\pi T^3}{2m_\rho^3}} \\ \times \left\{ \left[ \int_{(m_\rho+M)^2}^\infty ds e^{-\frac{s+m_\rho^2-M^2}{2m_\rho T}} + \int_0^{(m_\rho-M)^2} ds e^{-m_\rho/T} \right] \int_{u_-}^{u_+} du + 2 \mathbf{P} \int_{m_\rho^2}^\infty dt e^{-\frac{t+m_\rho^2}{2m_\rho T}} \int_{u_{\min}}^{u_{\max}} du \right\} \\ \times \left[ 2 + \frac{m_\rho^2 M^2}{4} \left( \frac{1}{t^2} + \frac{1}{u^2} \right) + \frac{(m_\rho^2 + M^2)^2 + m_\rho^2 M^2 / 2}{tu} - (m_\rho^2 + M^2) \left( \frac{1}{t} + \frac{1}{u} \right) \right], \quad (2.12)$$

where

$$\begin{aligned} u_{(-)}^{\pm} &= \frac{1}{2} (m_\rho^2 + M^2 - s) \begin{pmatrix} + \\ - \end{pmatrix} \frac{1}{2} \sqrt{(s - (m_\rho + M)^2)(s - (m_\rho - M)^2)}, \\ u_{\max} &= m_\rho^2 M^2 / t, \quad u_{\min} = m_\rho^2 + M^2 - t, \end{aligned} \quad (2.13)$$

with  $s + t + u = m_\rho^2 + M^2$ . The  $u$ -integration may still be performed analytically.

The kinematic boundaries of integration given for the processes, which are summed in (2.12) in the order of  $\pi\pi \rightarrow \rho\gamma^*$ ,  $\rho \rightarrow \pi\pi\gamma^*$ ,  $\pi\rho \rightarrow \pi\gamma^*$ , are illustrated in the Mandelstam plot of Fig. 8.

The result contained in (2.12), for the squared matrixelements of Fig. 4, is successfully compared with the one derived in [14] for the case of the two-body processes involving a real photon.

It is important to note that due to the non-vanishing  $\rho$  mass and the heavy photon,  $M > 0$ , no mass singularities appear in (2.12), even when setting the  $T = 0$  pion mass to zero. However, for the evaluation of the  $\pi\rho \rightarrow \pi\gamma^*$  contribution, the principal value prescription leading to a well defined integral, e.g. in (2.12)  $\mathbf{P}(1/u) \equiv \lim_{\varepsilon \rightarrow 0} u/(u^2 + \varepsilon^2)$ , and correspondingly for  $\mathbf{P}(1/u^2)$  [18], has to be taken into account, in order to correctly treat the behaviour near  $u \simeq 0$ , which is covered by the kinematical domain of this process (Fig. 8). For the processes  $\pi\pi \rightarrow \rho\gamma^*$  and  $\rho \rightarrow \pi\pi\gamma^*$  the  $\mathbf{P}$  prescription is not explicitly required.

We plot the rate (2.12) below the  $\rho$ -peak in Fig. 5 as a function of the dilepton mass  $M$  for  $M \geq 0.2$  GeV at fixed temperature  $T = 150$  MeV. For comparison the Born rate  $\pi\pi \rightarrow \gamma^*$  is also included. We find that, as expected, the two-body reactions  $\pi\pi \rightarrow \rho\gamma^*$  and  $\pi\rho \rightarrow \pi\gamma^*$ , together with the decay channel  $\rho \rightarrow \pi\pi\gamma^*$ , dominate the dilepton rate for low masses<sup>1</sup>. Thus, when discussing the thermal yield in the context of recent experimental data on dilepton production in heavy ion collisions, it is necessary to include the above higher order processes.

It is worth to mention that admitting in-medium effects on the  $\rho$  meson mass or width, as recently proposed in Refs. [7, 9, 10], could substantially influence the overall thermal rate (solid curve) shown in Fig. 5. In particular, assuming a decrease of the  $\rho$  meson mass by only 100 MeV would imply an increase of the thermal rate (solid curve of Fig. 5) by a factor of 2.

### 2.2.2 Virtual $\rho^0$ processes

For heavy photon production at  $O(g_\rho^2)$  we have, in order to correct the Born rate (2.6), to include virtual contributions, which arise from the processes shown in Figs. 2 and 3 by cutting the diagrams in the proper way only through pion lines, without cutting the  $\rho$  line. For the production of real photons [14] these contributions are absent.

In some detail we describe our estimate, including the approximations, for the selfenergy diagram (Fig. 2). Here we take the first term of (B.5) and evaluate (cf. 2.9),

$$i\delta\Pi_{12}^{\gamma, virtSE}(q^0, \vec{q}) = (-ie)^2 \int \frac{d^4 p'}{(2\pi)^3} (p + p')^2 \epsilon(p_0) n(p_0) \delta'(p^2) \text{Re}\Pi(p) iD_{21}(p'), \quad (2.14)$$

---

<sup>1</sup>We note that the curves do not strongly change when the kinematical approximations performed in Appendix D are relaxed, e.g. for  $\pi\pi \rightarrow \rho\gamma^*$  at most a 10% change is numerically found when the  $\rho$  is not kinematically kept fixed at rest

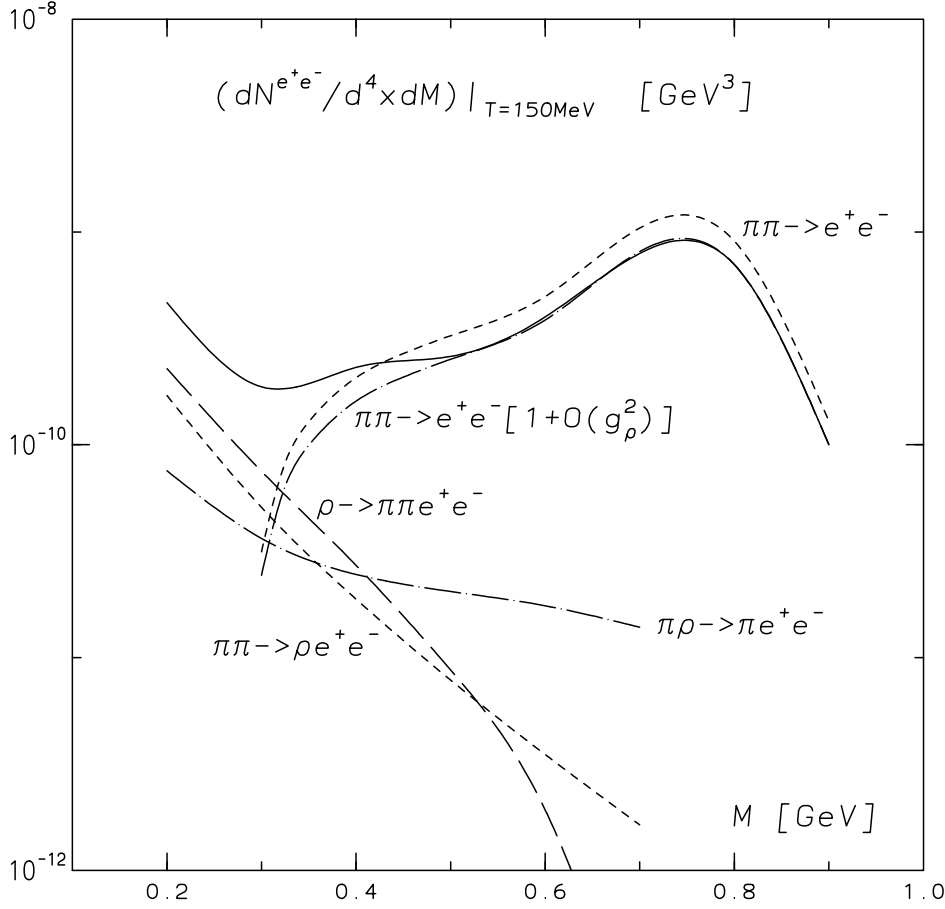


Figure 5: Dilepton rate as a function of  $M$  at fixed  $T = 150$  MeV. The solid curve represents the sum of the real and the virtual processes

where now the real part of the pion selfenergy  $\Pi(p)$  enters, and equilibrium distributions are used.

The temperature-independent part of  $\text{Re}\Pi$  is absorbed in the definition of the  $T = 0$  pion mass (which we take approximately as  $m_\pi = 0$ ). The temperature dependent part in the one-loop case under consideration is weighted by the thermal distribution either for the  $\rho$  meson or for the pion (see [13]). The first case is of  $O(\exp(-m_\rho/T))$ , i.e. negligible, the second one therefore dominates and is expected to be of  $O(T^2/m_\rho^2)$ , due to the presence of the  $T = 0$   $\rho$ -propagator in the loop (Fig. 2).

In the following we estimate (2.14) in the limit  $m_\rho \gg T$ , having in mind the mass region  $M \leq m_\rho$ . To obtain the result analytically we make the further simplifying assumption of dileptons at rest (cf. (2.5)). Then it is straightforward to find

$$i\delta\Pi_{12}^{\gamma, \text{virt}SE}(M, \vec{q} = 0) = e^2 \int \frac{d^3p'}{(2\pi)^2} \frac{1}{2E'} n(E') n(M - E') \delta'(M/2 - E') (E'/M - 1/4) \text{Re}\Pi(M - E', -\vec{p}'), \quad (2.15)$$

where  $|\vec{p}'| = E'$ .



When evaluating  $\text{Re}\Pi(p_0, \vec{p})$  on-shell, we get

$$\text{Re}\Pi(M/2, \vec{p}) \simeq O(M^2 (T/m_\rho)^4), \quad (2.16)$$

for  $|\vec{p}| = M/2$ , and therefore it will be neglected. The leading term of (2.15) is found after partial integration with respect to the variable  $E'$ ; it is proportional to the derivative

$$\frac{\partial}{\partial E'} \text{Re}\Pi \simeq -\frac{g_\rho^2}{4\pi^2} M \frac{T^2}{m_\rho^2}, \quad (2.17)$$

when evaluated on-shell because of the  $\delta$ -function constraint in (2.15), and using Boltzmann distributions. As expected we obtain

$$i\delta\Pi_{12}^{\gamma, \text{virtSE}}(M, \vec{q}=0) \simeq -\frac{e^2}{8\pi^2} \frac{g_\rho^2}{4\pi} M^2 \frac{T^2}{m_\rho^2} \exp(-M/T), \quad (2.18)$$

where we already include a factor 2 for the diagram Fig. 2 after interchanging  $p$  with  $p'$ .

In an analogous treatment we evaluate the virtual  $T$ -dependent contributions from the vertex type diagrams, namely from the first two of Fig. 3. After a lengthy calculation the result is

$$\begin{aligned} \frac{dN^{\text{Born+virtual}}}{dM^2 d^4x} &\simeq \\ \frac{dN^{\text{Born}}}{dM^2 d^4x} &\left[ 1 + \frac{g_\rho^2}{4\pi} \left(\frac{T}{m_\rho}\right)^2 \left(-\frac{19}{3\pi} + \frac{M^2}{6\pi T^2} \mathbf{P} \int_0^\infty n(k) \frac{kdk}{(k^2 - M^2/4)}\right) \right] \simeq \\ &\frac{dN^{\text{Born}}}{dM^2 d^4x} \left[ 1 - \frac{7}{\pi} \frac{g_\rho^2}{4\pi} \left(\frac{T}{m_\rho}\right)^2 \right], \end{aligned} \quad (2.19)$$

valid for  $m_\rho \gg T$ , and for  $M > 0$ .

In Fig. 5 we see that e.g. for  $T = 150$  MeV the  $T$ -dependent virtual corrections (2.19) are negative and rather large. It suggests to perform resummations, which, however, we do not attempt.

### 3 Out of equilibrium effects

In the early stage of heavy ion collisions, when lepton pairs are expected to be predominantly produced [1, 2, 3, 4], it is more likely that the pion gas is not yet in thermal and chemical equilibrium [25, 26]. Before we treat the realistic situation of an expanding gas in the next section, we first have to compute the production rate using non-equilibrium distributions, thus generalizing the calculation of sect. 2. We proceed with a tractable, but still realistic ansatz [25, 26] by introducing the fugacity parameter [27]  $\lambda$  and by using the following distributions<sup>2</sup>  $\tilde{n}(|k_0|) \simeq \lambda e^{-|k_0|/T}$  in Boltzmann approximation (cf. (A.6) and (A.7)). We have in mind that  $\delta\lambda \equiv \lambda - 1$  is small  $\delta\lambda \ll 1$ , i.e. a situation not far off equilibrium, in order to be consistent with the simplifying approximations summarized in Appendix A.

---

<sup>2</sup>We do not distinguish the fugacity parameter for  $\pi^\pm$  and  $\rho$  respectively

In order to estimate non-equilibrium effects even under these approximations it is not justified to simply multiply the real emission rate (2.12) by a factor  $(1 + 2\delta\lambda)$  as it is in the case of the Born rate (cf. (2.7)). Due to the structure of the (one-loop) selfenergy correction to the pion propagator (B.3) a more careful derivation is required. For the real emission contribution it first amounts to the replacement of (2.9) by

$$i\delta\Pi_{12}^{\gamma,off}(q^0, \vec{q}) \simeq -(-ie)^2 \int \frac{d^4p}{(2\pi)^4} (p+p')^2 \left\{ \mathbf{P}\left(\frac{1}{p^2}\right)^2 n(p_0) (i\Pi_{12}(p) - i\Pi_{21}(p)) \right. \\ \left. + \frac{1}{(p^2)^2 + (p_0\gamma)^2} (n(p_0)i\Pi_{21}(p) - (1+n(p_0))i\Pi_{12}(p)) \right\} iD_{21}(p'), \quad (3.1)$$

where again a corresponding term with  $(p \leftrightarrow p')$  has to be added. In the second term in (3.1) the pinch singularity, which is not cancelled in case of non-equilibrium distributions [28], is regularized [29] by the damping rate  $\gamma$  of the pion, which we estimate in Appendix C. The expression for  $i\Pi_{12}(p)$  is the same as in (2.10), except that it now has to be evaluated using the non-equilibrium distributions (A.6), as it is the case for  $n(p_0)$  in (3.1).

We here discuss further details of the estimate for the dominant contribution, which is due to  $\pi\rho \rightarrow \pi\gamma^*$  in the limit  $\gamma \rightarrow 0$ , in order to exhibit our treatment, i.e. the regularization of the pinch singularities in the vicinity of  $t/u \simeq 0$  (cf. Fig. 8).

It is crucial to consider the following product of distributions, which is present in (3.1),

$$(1 + n(p'_0)) [n(p_0)n(k_0)(1 + n(p_0 + k_0)) - (1 + n(p_0))(1 + n(k_0))n(p_0 + k_0)] , \quad (3.2)$$

adjusted for the kinematics of the process  $\pi(p_{in}) + \rho(k_\rho) \rightarrow \pi(p_{out}) + \gamma(q)$ , i.e.  $p' \rightarrow -p_{in}, k \rightarrow -k_\rho, p \rightarrow -p_{out} + k_\rho$  (cf. Fig. 2). In relation to the definitions (D.4) we have to continue:  $k \rightarrow -k_\rho, p_+ \rightarrow -p_{out}, p_- \rightarrow p_{in}$ , which corresponds to the physical region (ii) with  $u \geq m_\rho^2$  in Fig. 8. The limit  $\gamma \rightarrow 0$  is sensitive to the behaviour near  $t = (k_\rho - p_{out})^2 \simeq 0$ . In the simplifying kinematical approximation of the  $\rho$ -meson at rest,  $E_\rho \simeq m_\rho$ , used in Appendix D, the region  $t \simeq 0$  corresponds to positive energy  $p_0 \simeq \frac{t+m_\rho^2}{2m_\rho} > 0$ .

Thus the product of distributions (3.2) reads in the Boltzmann approximation,

$$-\lambda^2(\lambda - 1)e^{\frac{E_\rho + E_{out}}{T}} \simeq -\delta\lambda e^{-\frac{u+m_\rho^2}{2m_\rho T}} \quad (3.3)$$

valid for  $p_0 > 0$  and in leading order of  $\delta\lambda$ . The dominant contribution arising from (3.1) to the dilepton spectrum becomes

$$\frac{dN^{pinch}}{dM^2 d^4x} \stackrel{\gamma \rightarrow 0}{\simeq} -\delta\lambda \frac{\alpha^2(g_\rho^2/4\pi)}{48\pi^4 M^2} \sqrt{\frac{\pi T^3}{2m_\rho^3}} \\ \times \left\{ \int_{m_\rho^2}^{2m_\rho^2 + M^2} du e^{-\frac{u+m_\rho^2}{2m_\rho T}} \int_{t_{min}}^{t_{max}} dt + \int_{2m_\rho^2 + M^2}^\infty du e^{-\frac{u+m_\rho^2}{2m_\rho T}} \int_{-m_\rho^2}^{t_{max}} dt \right\} \frac{m_\rho^2 M^2}{t^2 + \left[\frac{g_\rho^2 T^2}{4\pi e}\right]^2}, \quad (3.4)$$

where we take into account by a factor of 2 both regions denoted by (ii) in Fig. 8. The boundaries of the integrations are defined as in (2.13), except for  $t \leftrightarrow u$ . When using in (3.4) the momentum independent value for the damping  $\gamma$  (C.5) the integrations can be explicitly performed. The leading term with  $\gamma \rightarrow 0$  is proportional to  $1/\gamma$ , indicating the pinch singularity,

$$\frac{dN^{pinch}}{dM^2 d^4x} \simeq -\delta\lambda \frac{\alpha^2(g_\rho^2/4\pi)}{24\pi^3} \sqrt{\frac{\pi T^3}{2m_\rho^3}} \frac{m_\rho^3}{g_\rho^2/(4\pi e)T} e^{-\frac{2m_\rho^2 + M^2}{2m_\rho T}}, \quad (3.5)$$

which is actually independent of the coupling  $g_\rho^2$ . From Fig. 8 one can read off that the pinch near  $t \simeq 0$  is present starting at  $u \geq m_\rho^2 + M^2$ . This and (3.3) explains the argument of the exponential function in (3.5).

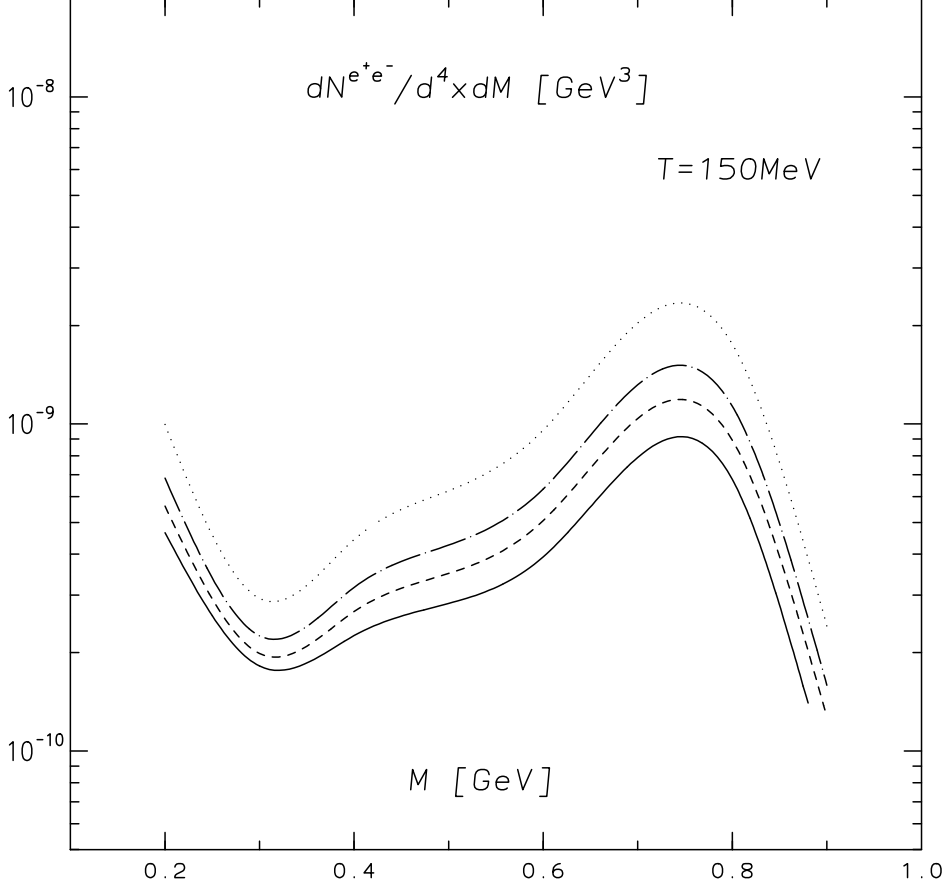


Figure 6: *Estimates of out of equilibrium effects to the dilepton rate up to  $O(g_\rho^2)$  at fixed  $T = 150$  MeV: solid curve corresponds to  $\mu = 0$ , dashed to  $\mu = 25$ , dashed-dotted to  $\mu = 50$ , and dotted to  $\mu = 100$  MeV, respectively*

We remark that (3.5) differs numerically by only a few percent from the more exact expression starting from (3.1) and including all the contributions due to the processes (i) - (iii) defined in Appendix D.

In Fig. 6 we plot the total rate  $dN/dM d^4x$ , including the Born term with  $O(g_\rho^2)$  correction, for non-equilibrium cases characterized by different values of the chemical potential  $\mu$ , including even as large values as  $\mu = 100$  MeV, which corresponds to a large value of  $\lambda \simeq 1.95$  at  $T = 150$  MeV. Although here  $\delta\lambda$  may be considered too large to justify keeping only  $O(\delta\lambda)$  terms<sup>3</sup>, as done in the calculation of the curves plotted in Fig. 6, we observe that instead of an expected increase by a factor of  $\lambda^2 \simeq 4$ , only an effective increase of the rate by a factor 2 results, because of the negative contribution estimated in (3.5), when we change  $\mu$  from  $\mu = 0$  to  $\mu = 100$  MeV. From this fact we stress the importance of taking into account the non-trivial term (3.1), which

<sup>3</sup> A different estimate in case of large  $\lambda$ , namely replacing  $\gamma \rightarrow \lambda\gamma$ , and  $Born(1 + O(g_\rho^2)) \rightarrow \frac{\lambda^2 B_{\text{Born}}}{(1 - O(\lambda g_\rho^2))}$ , etc. actually gives the same result as in Fig. 6

is traced back to the selfenergy diagram (Fig. 2). For completeness we state that no such extra terms arise from the vertex type diagrams of Fig. 3.

## 4 Soft dileptons in the expanding hadronic medium

In the previous sections we have derived the dilepton production rate originating from  $\pi - \rho$  interactions up to  $O(g_\rho^2)$  in a thermal medium as a function of temperature and for fixed chemical potential. In the description of dilepton spectra in heavy ion collisions we have in addition to take into account that dilepton pairs are emitted from a rapidly expanding and thereby cooling medium. Hot hadronic matter produced in heavy ion collisions undergoes an expansion, which leads to a space-time dependence of the thermal parameters. In the expanding system we therefore have to integrate the rates derived in the previous sections over the space-time history of the collision. As a model for the expansion dynamics we assume the Bjorken model for 1+1 dimensional longitudinal hydrodynamical expansion [30]. In this model all thermodynamical parameters are only a function of the proper time,  $\tau$ , and do not depend on the rapidity variable,  $y$ . We furthermore assume, that at some initial time  $\tau_0 \sim 1$  fm matter is formed as a thermalized hadronic gas with initial temperature  $T_0$ . The system subsequently expands and cools until it reaches the freeze-out temperature of  $T_f \sim 130$  MeV. We have modeled the hadronic gas equation of state with a resonance gas where all hadrons and resonance states with masses up to 2.5 GeV are included. The value of the initial temperature  $T_0 \simeq 210$  MeV has been fixed by the requirement to reproduce the multiplicity of 150 charged pions in the final state at central rapidity. These numbers are for S-Au collisions [5].

With the above defined model for the expansion dynamics the space-time integration of the rates, first calculated in equilibrium, namely the Born rate including the virtual correction of  $O(g_\rho^2)$  (2.19), and the real processes (2.12), can be performed leading to the spectrum which may then be compared with the one experimentally measured in heavy ion collisions. In Fig. 7 we show the overall thermal dilepton rate from  $\pi - \rho$  interactions including acceptance and kinematical cuts of the CERES experiment [5]. One can see in Fig. 7 that with the thermal source for dielectron pairs due to  $\pi - \rho$  interactions discussed in sect. 2 one can partially account for the excess reported by the CERES Collaboration as measured in S-Au (and Pb-Au) collisions. This is particularly the case in the vicinity of the  $\rho$  peak where the agreement with the experimental data is quite satisfactory. However, the enhancement below the  $\rho$  peak and the structure of the distribution can not be explained by equilibrium production alone. In the kinematical window  $0.25 < M < 0.45$  GeV there are still almost 70% deviations of our theoretical curve from the experimental results. Assuming non-chemical equilibrium in the mesonic medium (as discussed in sect. 3) should certainly increase the dilepton rate. This is mostly because, in this case, there are more soft pions and rho mesons, which should produce more abundant soft dileptons. In Fig. 7 we show the thermal rate (long-dashed curve) assuming deviations from chemical equilibrium with the value of the chemical potential  $\mu = 100$  MeV. Indeed, we observe an increase of the rate below the rho peak. This increase, however, is rather modest particularly in the soft part of the spectrum. The main reason is due to the "pinch singular" term (3.5), which being negative reduces the contributions of the two-loop processes, when considered out of equilibrium. In addition the out of equilibrium distributions of pions and rho mesons lead to a lower initial temperature and a shorter lifetime of the thermal system. All these effects are the reason of small modifications of the dilepton yield.

Here, also additional assumptions e.g. on in-medium effects of the  $\rho$  meson mass and width eventually help to understand more completely the dilepton access measured by the CERES Collaboration [7, 9, 10].

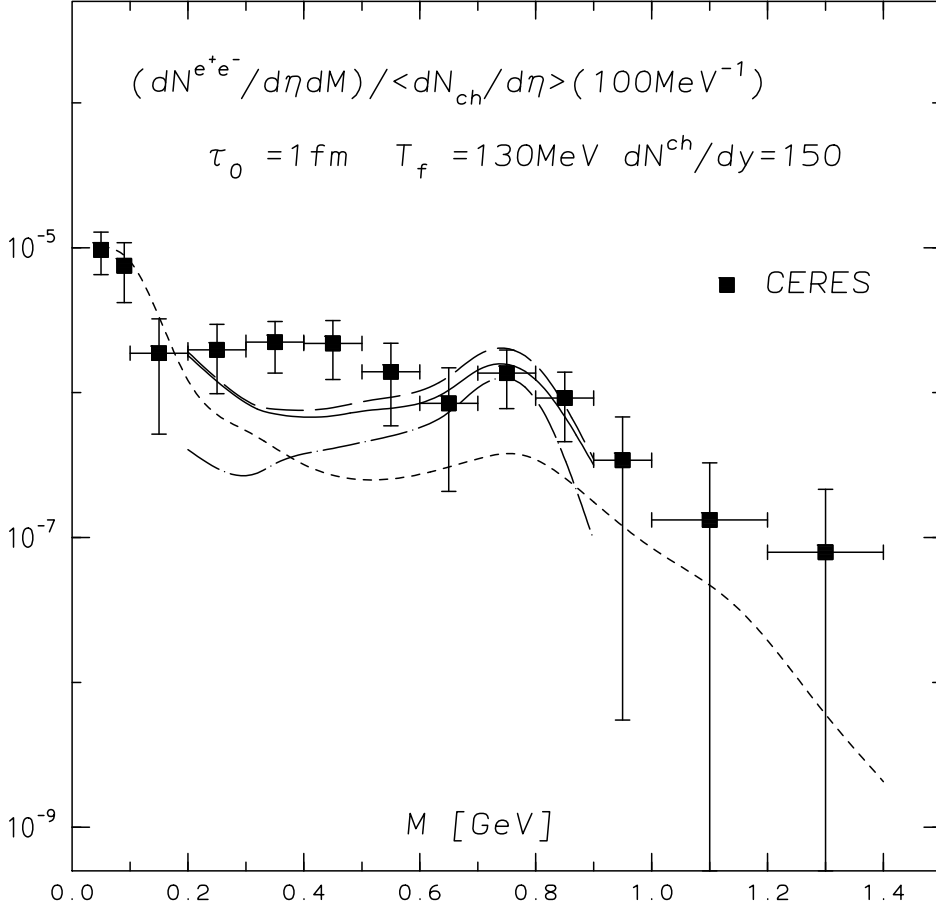


Figure 7: *Invariant-mass dielectron spectra measured by the CERES Collaboration for the S-Au collisions [5] in comparison with the thermal yield from  $\pi - \rho$  interactions. Dashed-dotted line describes the sum of all contributing reactions from  $\pi^\pm - \rho^0$  interactions. The dashed line, calculated by CERES, represents the expected dielectron yield from all known hadronic sources. The full-line is the sum of the contributions described by the dashed-dotted and dashed curves. The long-dashed curve includes the out of equilibrium effects*

## 5 Summary

We have calculated the thermal production rate for soft dielectrons produced in a pion gas including relevant reactions from  $\pi - \rho$  interactions. The calculations include the  $O(g_\rho^2)$  corrections arising from the two-loop contributions to the virtual photon selfenergy. The dilepton rate is first calculated using equilibrium distributions. Next off equilibrium contributions to the rates have been estimated. Finally, dilepton production in an expanding hadronic medium has been calculated applying the Bjorken model. No medium effects on the  $\rho$  resonance parameters are included in the analysis. The access reported by the CERES Collaboration in the low mass range below the  $\rho$  peak is diminished, although not yet completely described by the model.

## Acknowledgements

One of us K. R. acknowledges stimulating discussion with members of the CERES Collaboration and partial support of the Gesellschaft für Schwerionenforschung (GSI) and of the Committee of Research Development (KBN 2-P03B-09908). Supported in part by the EEC Programme "Human Capital and Mobility", Network "Physics at High Energy Colliders", Contract CHRX-CT93-0357. M. D. is supported by DFG.

## Appendix A: Thermal propagators

In order to perform the perturbative calculations presented in this paper we use the closed-time-path formalism of thermal field theory [18, 19, 20]. The real-time  $2 \times 2$  matrix (scalar) propagators,

$$\begin{aligned} D_{11}(k) &= (1 + n(k_0))\Delta_R(k) - n(k_0)\Delta_A(k), \\ D_{12}(k) &= n(k_0)(\Delta_R(k) - \Delta_A(k)), \\ D_{21}(k) &= (1 + n(k_0))(\Delta_R(k) - \Delta_A(k)), \\ D_{22}(k) &= n(k_0)\Delta_R(k) - (1 + n(k_0))\Delta_A(k), \end{aligned} \quad (\text{A.1})$$

are expressed in terms of the retarded and advanced propagators,

$$\Delta_{R(A)}(k) = \frac{1}{k^2 - m^2 \begin{smallmatrix} + \\ - \end{smallmatrix} i\epsilon k_0}, \quad (\text{A.2})$$

where  $k^2 = k_0^2 - \vec{k}^2$  and  $m$  is the  $T = 0$  mass. For equilibrium conditions the Bose-Einstein distribution function  $n(k_0)$  depends on temperature  $T$ ,

$$n(k_0) = \frac{1}{e^{k_0/T} - 1}, \quad (\text{A.3})$$

and satisfies

$$n(k_0) + n(-k_0) + 1 = 0. \quad (\text{A.4})$$

For our numerical estimates we are mainly using the Boltzmann approximation

$$n(|k_0|) \simeq \exp(-|k_0|/T). \quad (\text{A.5})$$

Estimating non-equilibrium effects we follow the approximations described in detail in [19], and more recently in [31]. It amounts to replace the thermal  $n(k_0)$ , (A.3), by their non-equilibrium counter parts, i.e. in general by Wigner distributions  $n(k_0, X)$ . This corresponds in terms of the cumulant expansion to approximate non-equilibrium correlations by the second cumulant only. As a further approximation we suppress the possible dependence on the center of mass coordinate  $X$ , essentially assuming a homogenous and isotropic medium.

Practically for our estimates we take (cf. (A.4)),

$$n(k_0, X) \rightarrow \begin{cases} \tilde{n}(|k_0|) & k_0 > 0, \\ -(1 + \tilde{n}(|k_0|)) & k_0 < 0, \end{cases} \quad (\text{A.6})$$

with

$$\tilde{n}(|k_0|) \equiv \frac{1}{e^{(|k_0| - \mu)/T} - 1} \hat{=} \frac{\lambda}{e^{|k_0|/T} - \lambda}, \quad (\text{A.7})$$

by introducing the fugacity parameter [27]  $\lambda \equiv e^{\mu/T}$ , which is assumed to be energy independent. Obviously  $\lambda \neq 1$  in case of (chemical) non-equilibrium. Consequently deviations from equilibrium are approximated in terms of the equilibrium distribution (A.3) by

$$\frac{\delta n}{n(k_0)} \equiv n(k_0, X)/n(k_0) - 1 \simeq \delta\lambda \epsilon(k_0) (1 + n(k_0)) \quad (\text{A.8})$$

in leading order of  $\delta\lambda \equiv \lambda - 1$ .

In the expressions for  $\Delta_{R(A)}(k)$  the usual limit  $\epsilon \rightarrow 0$  is considered, whenever this limit is defined, e.g.

$$\Delta_R(k) - \Delta_A(k) = -2\pi i \epsilon(k_0) \delta(k^2 - m^2), \quad (\text{A.9})$$

where  $\epsilon(k_0) = \theta(k_0) - \theta(-k_0)$  is the sign function.

However, out of equilibrium pinch singularities appear in this limit  $\epsilon \rightarrow 0$  [28], e.g. in products like  $\Delta_R(k)\Delta_A(k)$  (see Appendix B). We treat this situation by following the conjecture by Altherr [29, 32] keeping  $\epsilon$  non-vanishing: it is identified by the damping width  $\gamma > 0$  (Appendix C).

## Appendix B: One-loop selfenergy correction to the pion propagator

Here we comment (cf. Fig. 2) on the selfenergy correction of the pion propagator and the possible appearance and presence of pinch singularities [18, 28]. Denoting the selfenergy insertion by the matrix  $\Pi_{ab}(p)$  we obtain the improved (12)-propagator using the Dyson equation,

$$\begin{aligned} iD_{12}(p) &\rightarrow iD_{12}(p) + \sum_{a,b=1,2} iD_{1a}(p)(-i\Pi_{ab}(p))iD_{b2}(p) \\ &= iD_{12}(p) + i\delta D_{12}(p). \end{aligned} \quad (\text{B.1})$$

With the propagators specified in the Appendix A, and with the relations

$$\Pi_{11}(p) = -\Pi_{22}^*(p), \quad \text{Im } \Pi_{11} = \frac{i}{2}(\Pi_{12} + \Pi_{21}), \quad (\text{B.2})$$

also valid out of equilibrium, we obtain

$$\begin{aligned} \delta D_{12}(p) &= n(p_0)(\Delta_R^2(p) - \Delta_A^2(p))\text{Re } \Pi_{11}(p) \\ &+ \frac{1}{2}n(p_0)(\Delta_R^2(p) + \Delta_A^2(p))[\Pi_{12}(p) - \Pi_{21}(p)] \\ &+ \Delta_R(p)\Delta_A(p)[n(p_0)\Pi_{21}(p) - (1 + n(p_0))\Pi_{12}(p)]. \end{aligned} \quad (\text{B.3})$$

Here the ill-defined product  $\Delta_R(p)\Delta_A(p)$  appears, giving rise to possible unpleasant pinch singularities [18, 28]. In case of equilibrium, however, it is well known that the last term in (B.3) vanishes due to the detailed balance condition,

$$\Pi_{21}(p) = e^{p_0/T} \Pi_{12}(p). \quad (\text{B.4})$$

As a consequence (B.3) simplifies to

$$\delta D_{12}^{eq}(p) = 2\pi i \epsilon(p_0) n(p_0) \left[ \delta'(p^2) \text{Re } \Pi(p) + \frac{1}{\pi} \mathbf{P} \left( \frac{1}{p^2} \right)^2 \text{Im } \Pi(p) \right], \quad (\text{B.5})$$

where

$$\text{Re } \Pi(p) \equiv \text{Re } \Pi_{11}(p), \quad \text{Im } \Pi \equiv \frac{1}{2} \epsilon(p_0) \frac{i\Pi_{12}(p)}{n(p_0)}, \quad (\text{B.6})$$

expressed in terms of the equilibrium distribution  $n(p_0)$ , and in terms of the (retarded) self-energy  $\Pi(p_0 + i\epsilon p_0, \vec{p})$  [23].  $\delta'$  denotes the derivative of the  $\delta$ -function, and  $\mathbf{P}$  the principal value.

However, for nonequilibrium distributions (A.6), for which obviously  $(1+n)/n \neq \exp(p_0/T)$ , the last term in (B.3) does not cancel! In order to regularize the product  $\Delta_R(p)\Delta_A(p)$  [29] we take into account the non-vanishing (on-shell) damping rate of the pion, which we estimate in the following Appendix C.



## Appendix C: Estimate of the damping rate of the pion

The pion damping rate  $\gamma$  is determined by the “pole” (in the lower energy half-plane) of the retarded propagator. In the following we not only neglect the pion mass, but also thermal corrections due to the real part of the (retarded) pion selfenergy, such that

$$\gamma \simeq -\frac{\text{Im } \Pi(p_0, \vec{p})}{p_0}, \quad (\text{C.1})$$

evaluated on-shell  $p^2 = 0$  for positive pion energy  $p_0$ . In the one-loop approximation the absorptive part of the pion selfenergy is given by

$$\text{Im } \Pi(p_0, \vec{p}) = \frac{g_\rho^2}{2n(|p_0|)} \int \frac{d^4 k}{(2\pi)^4} (2p+k)^\sigma \left( -g_{\sigma\tau} + \frac{k_\sigma k_\tau}{m_\rho^2} \right) (2p+k)^\tau D_{12}(p+k) D_{21}(k), \quad (\text{C.2})$$

where the momentum labels of Fig. 2 are used.

The temperature dependent non-vanishing part for  $p^2 = p_0^2 - \vec{p}^2 = 0$ , becomes (cf. the derivation in [13]),

$$\text{Im } \Pi(p_0 = p, |\vec{p}| = p) = -g_\rho^2 m_\rho^2 \pi \int \frac{d^3 k}{(2\pi)^3} \frac{1}{2E_p 2E_\pi} [n(E_\pi) - n(E_\rho)] \delta(p - E_\rho + E_\pi), \quad (\text{C.3})$$

with the corresponding energies are  $E_\rho = \sqrt{\vec{k}^2 + m_\rho^2}$  and  $E_\pi = |\vec{p} + \vec{k}|$ .

The dominant contribution comes from the pion’s thermal distribution  $n(E_\pi)$ . In the Boltzmann approximation it leads to

$$\text{Im } \Pi(p_0 = p, p) \simeq -\frac{g_\rho^2}{4\pi} \frac{m_\rho^2}{4p} \int_{\frac{m_\rho^2}{4p}}^\infty n(E_\pi) dE_\pi \simeq -\frac{g_\rho^2}{4\pi} \frac{m_\rho^2 T}{4p} e^{-\frac{m_\rho^2}{4pT}}. \quad (\text{C.4})$$

$\text{Im } \Pi$  vanishes for  $\vec{p} = 0$ , and it has its maximum near  $p \simeq \frac{m_\rho^2}{4T}$ . We note that (C.4) gives a positive damping rate  $\gamma$ , as required. In order not to overestimate the contributions arising from the  $\Delta_R \Delta_A$  terms we take for the numerical estimates a momentum independent value, namely the one at the maximum,

$$p_0 \gamma \simeq -\text{Im } \Pi(p_0 \simeq p, p) \simeq \frac{g_\rho^2}{4\pi} \frac{1}{e} T^2. \quad (\text{C.5})$$

## Appendix D: Kinematic boundaries for the kinetic processes

The dilepton thermal rate receives contributions from the two-body processes  $\pi\pi \rightarrow \rho\gamma^*$  and  $\pi\rho \rightarrow \pi\gamma^*$ , and from  $\rho \rightarrow \pi\pi\gamma^*$ , for which we evaluate in the following the phase-space integral (2.11) including its kinematic constraints. The calculation is simplified using (i) Boltzmann distributions and (ii) the fact that  $m_\rho/T \gg 1$ : the  $\rho$ -meson is kept at rest in the medium. This allows to integrate the  $\rho$ ’s phase-space by

$$I_\rho \hat{=} \int \frac{d^3 k}{(2\pi)^3} \frac{1}{2E_\rho} e^{-E_\rho/T} \simeq \frac{T^2}{4\pi^2} \sqrt{\frac{\pi m_\rho}{2T}} e^{-m_\rho/T}, \quad (\text{D.1})$$

and to replace elsewhere  $E_\rho = \sqrt{\vec{k}^2 + m_\rho^2} \simeq m_\rho$ .

The remaining integrations are carried out as we explicitly show in the following for the channel  $\pi(p_+) + \pi(p_-) \rightarrow \rho(k) + \gamma^*(q)$ . We only consider the case of dilepton masses  $M \leq m_\rho$ .

The phase-space integral defined by

$$I \hat{=} \int \frac{d^3 q}{q_0} \int \frac{d^3 p_+}{(2\pi)^3 2E_+} \int \frac{d^3 p_-}{(2\pi)^3 2E_-} \int \frac{d^3 k}{(2\pi)^3 2E_\rho} e^{-E_\rho/T} (2\pi)^4 \delta^4(p_+ + p_- - k - q) \quad (\text{D.2})$$

is approximated by

$$I \simeq \frac{1}{4\pi^2} I_\rho \int \frac{d^3 p_+}{2E_+} \int \frac{d^3 p_-}{2E_-} \frac{1}{q_0} \delta(E_+ + E_- - m_\rho - q_0) \quad (\text{D.3})$$

with  $q_0 \simeq \sqrt{|\vec{p}_+ + \vec{p}_-|^2 + M^2}$ . The angular integrations in  $I$  can be done.

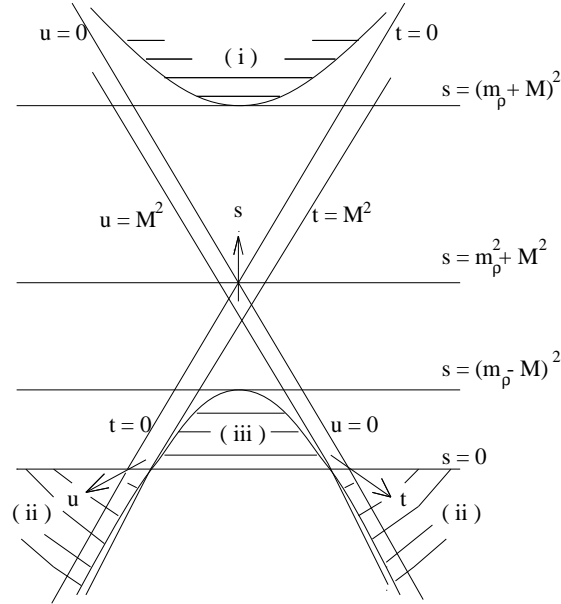


Figure 8: *Mandelstam plot: physical regions for the processes (i)  $\pi\pi \rightarrow \rho\gamma^*$ , (ii)  $\pi\rho \rightarrow \pi\gamma^*$  and (iii)  $\rho \rightarrow \pi\pi\gamma^*$*

Next we introduce the Mandelstam variables by

$$\begin{aligned} s &= (p_+ + p_-)^2 = (k + q)^2, \\ t &= (p_+ - k)^2 = (q - p_-)^2, \\ u &= (p_- - k)^2 = (q - p_+)^2, \end{aligned} \quad (\text{D.4})$$

with  $s + t + u = m_\rho^2 + M^2$ . Approximating the pion energies by

$$E_+ \simeq (m_\rho^2 - t)/2m_\rho, \quad E_- \simeq (m_\rho^2 - u)/2m_\rho, \quad (\text{D.5})$$

gives the final result for the phase-space integral,

$$I \simeq \frac{1}{8m_\rho^2} I_\rho \int dt du \theta(tu - m_\rho^2 M^2) \theta(s - (m_\rho + M)^2). \quad (\text{D.6})$$

The other channels only differ in their kinematical boundaries,

$$\begin{aligned}
(ii) \quad \pi\rho \rightarrow \pi\gamma^* & : \quad \theta(-s) \theta(m_\rho^2 M^2 - tu), \\
(iii) \quad \rho \rightarrow \pi\pi\gamma^* & : \quad \theta(s) \theta(tu - m_\rho^2 M^2),
\end{aligned}
\tag{D.7}$$

which are also summarized in Fig. 8. The processes  $\pi\pi\rho \rightarrow \gamma^*$  and  $\pi \rightarrow \pi\rho\gamma^*$  do not contribute due to the nonvanishing masses  $m_\rho$  and  $M$ .

We finally remark that the poles at  $t = 0$  and/or  $u = 0$  are present within the kinematical domain for the channel  $\pi\rho \rightarrow \pi\gamma^*$ , whereas for  $\pi\pi \rightarrow \rho\gamma^*$  they are present just at the kinematical boundary when  $s \rightarrow \infty$ .

## References

- [1] E. L. Feinberg, *Nuovo Cimento* **34A** (1976) 391;  
E. Shuryak, *Phys. Lett.* **78B** (1978) 150.
- [2] L. McLerran and T. Toimela, *Phys. Rev.* **D31** (1985) 545.
- [3] P. V. Ruuskanen, in *Quark-Gluon Plasma*, ed. R. Hwa (World Scientific, Singapore, 1990);  
J. Alam, S. Raha and B. Sinha, *Phys. Rep.* **273** (1996) 243.
- [4] J. Cleymans, K. Redlich and H. Satz, *Z. Phys.* **C52** (1991) 517.
- [5] CERES Collab., G. Agakichiev et al., *Phys. Rev. Lett.* **75** (1995) 1272;  
P. Holl et al., preprint CERN-SPSLC-95-35 (June 1996).
- [6] HELIOS/3 Collab., M. Maser, *Nucl. Phys.* **A590** (1995) 3c.
- [7] G. Q. Li, C. M. Ko and G. E. Brown, *Phys. Rev. Lett.* **75** (1995) 4007;  
W. Cassing, W. Ehehalt, C. M. Ko, *Phys. Lett.* **B363** (1995) 35.
- [8] D. K. Srivastava, B. Sinha and C. Gale, *Phys. Rev.* **C53** (1996) R567.
- [9] C. Adami and G. E. Brown, *Phys. Rep.* **224** (1993) 1;  
T. Hatsuda and S. H. Lee, *Phys. Rev.* **C46** (1992) R34;  
G. Q. Li and C. M. Ko, *Nucl. Phys.* **A582** (1995) 731;  
F. Karsch, K. Redlich and L. Turko, *Z. Phys.* **C60** (1993) 519;  
R. D. Pisarski, *Phys. Rev.* **D52** (1995) R3773.
- [10] C. Song, V. Koch, S. H. Lee and C. M. Ko, *Phys. Lett.* **B366** (1996) 379.
- [11] C. Gale and J. I. Kapusta, *Nucl. Phys.* **B357** (1991) 65; *Phys. Rev.* **C35** (1987) 2107.
- [12] C. Gale and P. Lichard, *Phys. Rev.* **D49** (1994) 3338.
- [13] C. Song, *Phys. Rev.* **D49** (1994) 1556; *Phys. Rev.* **D48** (1993) 1375.
- [14] J. I. Kapusta, P. Lichard and D. Seibert, *Phys. Rev.* **D44** (1991) 2774.
- [15] E. Braaten, R. D. Pisarski and T. C. Yuan, *Phys. Rev. Lett.* **64** (1990) 2242;  
S. M. H. Wong, *Z. Phys.* **C53** (1992) 465.
- [16] H. A. Weldon, *Phys. Rev.* **D42** (1990) 2384.
- [17] H. A. Weldon, *Phys. Rev.* **D28** (1983) 2007;  
R. L. Kobes and S. W. Semenoff, *Nucl. Phys.* **B260** (1985) 714.
- [18] N. P. Landsman and Ch. G. van Weert, *Phys. Rep.* **145** (1987) 141.
- [19] K.-C. Chou, Z.-B. Su, B.-L. Hao and L. Yu, *Phys. Rep.* **118** (1985) 1.
- [20] M. A. van Eijck and Ch. G. van Weert, *Phys. Lett.* **B278** (1992) 305.
- [21] K. L. Haglin, *Phys. Rev.* **C53** (1996) R2606;  
see also: C. M. Hung and E. V. Shuryak, preprint SUNY-NTG-96-16, hep-ph/9608299.

- [22] R. D. Pisarski, Phys. Rev. Lett. **63** (1989) 1129;  
E. Braaten and R. D. Pisarski, Nucl. Phys. **B337** (1990) 569;  
R. D. Pisarski, Nucl. Phys. **A525** (1991) 175c, and references therein.
- [23] M. Le Bellac, “*Thermal Field Theory*”, (Cambridge University Press, Cambridge, 1996),  
and references therein.
- [24] See, e.g. : R. Baier, B. Pire and D. Schiff, Phys. Rev. **D38** (1988) 2814;  
T. Altherr and P. Aurenche, Z. Phys. **C45** (1989) 99.
- [25] S. Gavin, Nucl. Phys. **B351** (1991) 561;  
S. Gavin and P. V. Ruuskanen, Phys. Lett. **B262** (1991) 326.
- [26] P. Koch, Z. Phys. **C57** (1993) 283;  
B. Kämpfer, P. Koch and O. P. Pavlenko, Phys. Rev. **C49** (1994) 1132.
- [27] S. R. de Groot, W. A. van Leeuwen and Ch. G. van Weert, “*Relativistic Kinetic Theory*”,  
(North Holland, Amsterdam, 1980);  
see also: T. S. Biro et al., Phys. Rev. **C48** (1993) 1275.
- [28] T. Altherr and D. Seibert, Phys. Lett. **B333** (1994) 149.
- [29] T. Altherr, Phys. Lett. **B341** (1995) 325.
- [30] J. D. Bjorken, Phys. Rev. **D27** (1983) 140.
- [31] M. Le Bellac and H. Mabilat, preprint INLN 96/17, July 1996.
- [32] For a discussion of pinch singularities, which differs from [29],  
P. F. Bedaque, Phys. Lett. **B344** (1995) 23.